Available online at www.sciencedirect.com
ScienceDirect
Journal of Catalysis 255 (2008) 127–133
JOURNAL OF CATALYSIS
www.elsevier.com/locate/jcat

Research Note

Identifying surface species by vibrational spectroscopy: Bridging vs monodentate nitrates

A. Desikusumastuti [a], T. Staudt [a], H. Grönbeck [b], J. Libuda [a,*]

[a] *Lehrstuhl für Physikalische Chemie II, Friedrich-Alexander-Universität Erlangen-Nürnberg, Egerlandstr. 3, D-91058 Erlangen, Germany*
[b] *Competence Centre for Catalysis, Chalmers University of Technology, SE-41296 Göteborg, Sweden*

Received 11 December 2007; revised 10 January 2008; accepted 21 January 2008

Available online 13 February 2008

Abstract

Identification of surface species by IR spectroscopy is often based on common knowledge, with a clear risk of misassignment. Combining density functional theory (DFT) and IR reflection absorption spectroscopy (IRAS), we investigated surface nitrate formation on BaO/Al_2O_3 thin films. We found that it is not possible to identify coordination geometries of nitrates based solely on their vibrational frequencies. For metal-supported thin films, however, differences in polarization of the NO stretching modes facilitate unambiguous identification. In contrast to traditional assignments, we show that both bridging and monodentate nitrates are formed on BaO, whereas on Al_2O_3 bridging nitrates dominate.

Keywords: Nitrogen dioxide; Barium oxide; Aluminum oxide; Density Functional Theory; IR reflection absorption spectroscopy; Supported model catalysts

1. Introduction

Infrared spectroscopy of adsorbates is among the most widely used experimental tools for both characterizing heterogeneous catalysts and investigating catalytic reaction mechanisms [1]. The reasons for this are simple: IR spectroscopy can be easily applied to many different types of samples, including powders or planar model catalysts [2,3], and provides unprecedented "chemical" resolution. Numerous surface intermediates are as easily identified by vibrational fingerprints as by their coordination geometry or specific adsorption sites [4–6].

But severe problems may arise when attempting to identify unknown surface species solely on the basis of their vibrational spectra. Traditionally, assignments are made on the basis of a pool of common knowledge that has evolved over many years from numerous experimental studies. In many cases, this knowledge can be traced back to comparisons with IR spectra of transition metal complexes containing similar ligands [5,7–9]. Unfortunately, the vibrational properties of complexes may differ substantially from those of adsorbed species on solid surfaces. In addition, the spectral regions of the characteristic bands may strongly overlap, impairing identification of different species. Consequently, in several cases, well-accepted assignments have been questioned and eventually discounted based on independent experiments or theoretical calculations, such as in the assignment of bonding sites of CO and NO on transition metal surfaces [4,10,11].

Whereas such independent experimental tests may be available for the ideal case of small molecules on single-crystal surfaces, the situation is less favorable for realistic catalytic reaction systems involving more complex surfaces and intermediates. In the present study, we focused on the formation and identification of nitrates on oxide surfaces, specifically Al_2O_3 and BaO. Recently, this reaction system has received much attention because of the application of Ba compounds in nitrogen storage and reduction (NSR) catalysts [12,13]. In brief, the NSR concept provides a potential strategy for removing NO_x from exhaust streams produced under lean-burn conditions. Such lean-burn engines (i.e., combustion engines operated under air-rich conditions) have substantially better fuel and CO_2 efficiency, but may have problems with respect to the emission of toxic gases, particularly NO_x. The NSR catalysts circumvent the difficulty of reducing NO_x under oxidizing conditions by

* Corresponding author. Fax: +49 9131 8528867.
E-mail address: libuda@chemie.uni-erlangen.de (J. Libuda).

0021-9517/$ – see front matter
doi:10.1016/j.jcat.2008.01.019

trapping NO_x in form of barium nitrates. Storage of NO_x during lean operation periods is followed by release and reduction of NO_x during short fuel-rich operation cycles.

Since it was first proposed by Toyota in 1996 [12], the NSR concept has attracted considerable attention [14–28]. Numerous attempts, most using diffuse reflectance infrared FT spectroscopy (DRIFTS), have been made to gain insight into the underlying reaction mechanisms; however, identifying the various nitrogen-oxo species involved is a demanding task, as demonstrated by the various contradictory assignments in the literature [15–18,21].

In this research note, we propose a method for identifying nitrogen-oxo species combining information on both the position of the bands and the polarization of the corresponding normal modes. Toward this aim, we combined IR reflection absorption spectroscopy (IRAS) on a model catalyst [2,29] and density functional theory (DFT) calculations. The NO_x storage model material was based on an ordered Al_2O_3 film prepared on a NiAl(110) single-crystal surface [30–33] on which BaO nanoparticles are grown under UHV (ultra-high vacuum) conditions [34]. This model approach reduces the complexity of the catalyst surface; moreover, the underlying metal allows us to obtain additional information on the polarization of vibrational modes with respect to the surface normal. Finally, comparison with DFT calculations allows clear identification of species, which would not be possible from the position of the vibrational bands only.

Using this approach, we show that, in contradiction to previous assignments, nitrates on BaO bind in both monodentate and bridging geometry. The ratio of both species depends on particle size, nitrate coverage, and reaction temperature. In contrast, only bridging nitrates are formed on the alumina support.

2. Experiments and theoretical calculations

The IRAS experiments were performed in an ultra-high-vacuum (UHV) system at the University Erlangen-Nuremberg. The MB/TR-IRAS (molecular beam/time-resolved IR reflection absorption spectroscopy) apparatus used allows superimposition of up to four effusive beams and one supersonic beam on the sample surface. In addition, the system is equipped with an FTIR spectrometer (Bruker IFS66/v) and numerous preparation and analysis tools. NO_2 (Linde, 99.0%) exposure was performed using an effusive beam doser. All measurements were performed by remote-controlled sequences, exposing the sample to pulses of NO_2 at variable beam intensity (corresponding to equivalent pressures between 1.2×10^{-7} and 1.4×10^{-5} mbar). NO_2 exposure was followed by acquisition of IR spectra (spectral resolution 2 cm^{-1}, typical acquisition time 38 s) at the corresponding reaction temperature. In this report, we show only selected spectra; a more detailed description of the reaction system and the results will be given in a forthcoming publication [35].

The Al_2O_3 film on the NiAl(110) surface was prepared as described previously [30,31]. For deposition of the BaO particles, the Ba metal was manually cleaned under an inert gas atmosphere (glove box), placed into a Mo crucible, and covered with decane to prevent oxidation [34]. The crucible was mounted into a commercial electron beam-assisted evaporator (Focus EFM3) in the UHV system, and the decane was pumped out. Under UHV conditions, the Ba source was calibrated using a quartz microbalance. During deposition, the sample was biased to the same potential as the Ba source, to avoid generation of surface defects by Ba ion bombardment. Ba was deposited at 300 K at typical rates of 1.0×10^{13} atoms cm^{-2} s^{-1} and then oxidized by exposure to 1×10^{-6} mbar O_2, at oxidation times of 90 s (0.125 MLE (monolayer equivalent) BaO) to 900 s (2.5 MLE BaO). Here we define a MLE based on the crystal structure of BaO (rock salt structure, lattice constant $a = 5.6$ Å, see [36]) as a layer with an average thickness of 5.6 Å, corresponding to a Ba^{2+} ion density of 1.26×10^{15} cm^{-2}. To avoid possible peroxide formation, the samples were annealed to 800 K in oxygen before being exposed to NO_2 [37].

DFT was applied with the gradient corrected exchange-correlation functional according to Perdew, Burke and Ernzerhof (PBE) [38]. The single-electron Kohn–Sham orbitals were expanded in a local numerical basis set [39,40]. In particular, a double numerical basis set was used together with polarization functions, and a real space cutoff of 10 Å was used for the basis functions. A pseudopotential [41] was used for Ba to describe the interaction between the valence electrons ($5s^2 5p^6 6s^2$) and the nucleus along with the inner shell electrons. The Kohn–Sham equations were solved self-consistently using an integration technique based on weighted overlapping spheres centered at each atom. The direct Coulomb potential was obtained by projecting the charge density onto angular-dependent weighting functions also centered at each atom, after which the Poisson equation was solved by one-dimensional integration. NO_x adsorption on BaO is known to have weak dependence on system size [42]; here we considered nitrite/nitrate pairs on a stoichiometric $(BaO)_9$ cluster as the model system. The investigated systems were structurally optimized, and vibrational analysis was performed via numerical derivatives.

3. Results and discussion

Recently, the structure and morphology of the BaO/Al_2O_3/NiAl(110) NO_x model storage system were characterized by scanning tunneling microscopy (STM) [34]. The insets in Fig. 1 show STM images of (i) the pristine Al_2O_3 film on NiAl(110) (top); (ii) smaller BaO particles on the Al_2O_3 film, corresponding to 0.125 MLE BaO (middle); and (iii) larger BaO particles on the Al_2O_3 film, corresponding to 2.5 MLE BaO (bottom). The pristine Al_2O_3 film is atomically flat and well ordered [30,31]. Recently, its structure was characterized by a combination of STM measurements and DFT calculations [32]. The bright lines correspond to a characteristic defect structure of antiphase domain boundaries, which also have been studied in detail [31,33].

After deposition of Ba and subsequent oxidation, small BaO particles are formed, which nucleate both on the oxide terraces and on the domain boundaries. From the particle density, as determined by STM, and the nominal BaO layer thickness, we

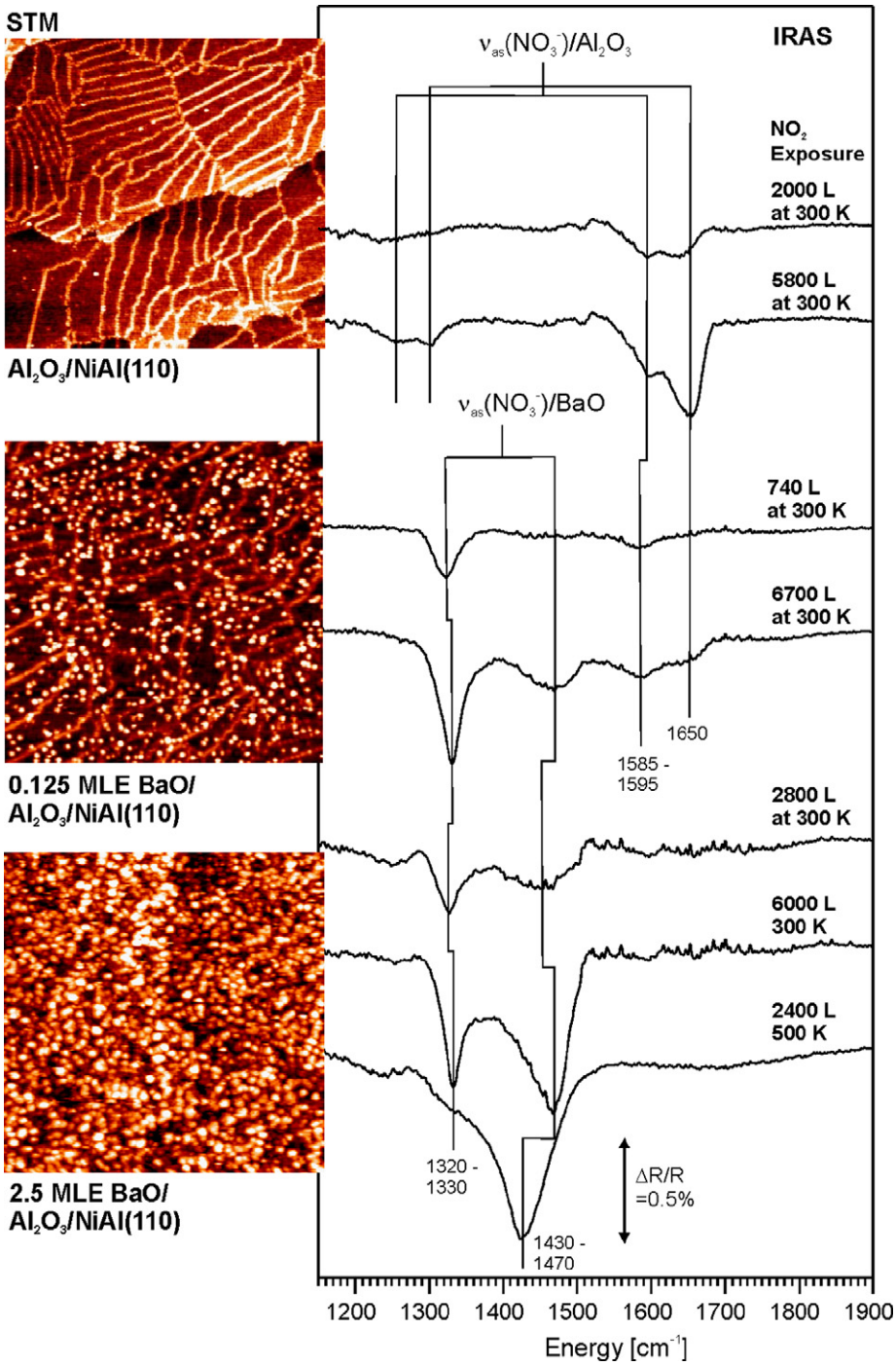

Fig. 1. Structure and vibrational properties of the model systems for NO_x storage. Left: STM images (200 × 200 nm^2), showing the pristine Al_2O_3 film on NiAl(110) (top), small BaO nanoparticles on the Al_2O_3 film (middle, $(BaO)_{\sim 30}$, 0.125 MLE BaO, see text), and large BaO nanoparticles on the Al_2O_3 film (bottom, $(BaO)_{\sim 600}$, 2.5 MLE BaO, see text). Right: IR reflection absorption spectra of the NO stretching frequency region after exposure to different doses of NO_2 (1 Langmuir (L) corresponds to 10^{-6} Torr s). The assignments of the bands are discussed in the text.

could derive an estimate of the average volume per BaO particle (see [34] for details). For the 0.125 MLE BaO, we obtained a volume of $(1.4 \pm 0.4) \times 10^{-27}$ cm^3 per particle, corresponding to approximately $(BaO)_{\sim 30}$, whereas for 2.5 MLE BaO, we obtained a volume of $(2.5 \pm 0.8) \times 10^{-26}$ cm^3, corresponding to approximately $(BaO)_{\sim 600}$. Determining particle shape was more difficult than determining particle density. STM yielded flat particles with an aspect ratio in a range of 6:1 to 5:1 (diameter:height). These values must be considered carefully, however, due to the varying electronic structures of the materials involved and convolution effects with the STM tip. Nevertheless, comparisons with previous STM studies of nanoparticles on the same support [43] suggest that even if these convolution effects are taken into account, the diameter of the particles is still much larger than their height; that is, the particles are rather flat.

Next, we considered the interaction of NO_2 with the three model surfaces. The reaction of NO_2 with BaO/Al_2O_3/NiAl(110) turned out to be a rather complex process, as we discuss in detail in a forthcoming publication [35]. In brief, various types of surface nitrites, surface nitrates, and ionic nitrates can be identified, depending on the reaction temperature and NO_2 exposure. The scenario can be summarized as follows [34,35]: At low NO_2 exposure, the formation of surface nitrites dominates for both the Al_2O_3/NiAl support and the BaO/Al_2O_3/NiAl. These surface nitrites give rise to weak bands at 1200–1300 cm^{-1} for both surfaces. This frequency range is in accordance with previous studies [16,18,21,44,45] and with the theoretical calculations presented below (see also [21]). The low intensity of the nitrite bands can be traced back to the flat-lying adsorption geometry of this species. As discussed below, the dynamic dipole moment of the flat-lying NO_2^- will be oriented nearly parallel to the surface, giving rise to only weak bands in IRAS. With continuing exposure, surface nitrates also are formed, followed by ionic nitrates in the limit of high exposure and temperature. Various mechanisms of nitrate formation, including disproportionation to nitrate–nitrite pairs [21,42,46], possibly via nitrosyl formation [44,47], have been discussed in the literature. Concerning the reaction mechanism, it also should be noted that for the present thin-film system, additional effects, such as oxidation of the support (leading to an increasing thickness of the oxide film [48]), may need to be taken into account. Surface nitrates typically are identified by characteristic bands due to the symmetric and the asymmetric NO-stretching modes $\nu_s(NO_3^-)$ and $\nu_{as}(NO_3^-)$. The symmetric mode $\nu_s(NO_3^-)$ appears at around 1000 cm^{-1} and is IR-forbidden in the gas phase; however, it may gain some intensity on interaction with the surface [5]. For the present model systems, the intensity of $\nu_s(NO_3^-)$ is generally very low, and the band can be identified in few favorable cases only. The asymmetric mode $\nu_{as}(NO_3^-)$ is characterized by a large dynamic dipole moment. In the free ion, the mode is twofold degenerate, but this degeneracy is lifted on interaction with the surface. The two components typically appear in a frequency range of 1200 and 1650 cm^{-1} [5]. Here we discuss the IR spectroscopic identification of surface nitrates through this split asymmetric NO-stretching mode.

Fig. 1 displays a selection of characteristic IR spectra of the NO-stretching frequency region. The spectra correspond to the three sample surfaces after exposure to NO_2 at different temperatures. All spectra are dominated by surface nitrate bands. For NO_2 on Al_2O_3, two weak bands at 1255 and 1297 cm^{-1} and two strong bands at 1590 and 1650 cm^{-1} are seen. These bands can be attributed to the asymmetric stretching vibration $\nu_{as}(NO_3^-)$ of surface nitrates on alumina [15,16,18–20,23,45]. The literature discusses various adsorption geometries, including monodentate nitrates and bridging nitrates (including bridging chelates) [45]. The "traditional" picture implies that the coordination geometry can be identified via the splitting of the two components of $\nu_{as}(NO_3^-)$, which is thought to be larger for the bridging nitrates than for the monodentate; however, in what follows, we demonstrate that this strict correlation is not valid in general.

Proceeding to the reaction of NO_2 with BaO/Al_2O_3, we observe that the alumina-derived bands are strongly attenuated or vanish completely at high BaO coverage. The weak band at around 1200–1250 cm^{-1} (Fig. 1; 2.5 MLE BaO) can be assigned to Ba nitrites and is not discussed here; however, it should be noted that despite the low intensity of these bands on IRAS, surface nitrites may be highly abundant [49]. We return to this point later. The dominating bands at around 1320–1330 cm^{-1} and 1430–1470 cm^{-1} can be attributed exclusively to surface nitrates on BaO, as shown in a recent X-ray photoelectron spectroscopy study [49]. Nitrate bands in these spectral regions on both BaO and on BaO/Al_2O_3 have been reported by various authors [15,16,18,21,23]. The splitting between the two components of the $\nu_{as}(NO_3^-)$ on BaO is substantially smaller than that between the nitrates on Al_2O_3; consequently, most authors have attributed the corresponding bands to a monodentate nitrate species.

To test the validity of these assignments, we performed DFT calculations for nitrite/nitrate pairs on $(BaO)_9$ clusters. Previous theoretical studies have revealed that nitrites or $[O_s–NO_2]^{2-}$ species (where O_s is a surface oxygen) are formed on adsorption of NO_2 on BaO [21]. It also has been demonstrated that subsequent NO_2 adsorption leads to the formation of nitrite/nitrate pairs [21]. These pairs can be of two kinds, NO_2^-–Ba^{2+}–$[O_sNO_2]^-$ and NO_3^-–Ba^{2+}–$[O_s–NO]^-$. Due to electron pairing, the adsorption energy per NO_2 is higher for the pairs than for NO_2 radicals.

Fig. 2 shows the relaxed structural models together with the calculated vibrational spectra. Three different models were studied: one model of type NO_2^-–Ba^{2+}–$[O_sNO_2]^-$ (Fig. 2, top panel) and two models of type NO_3^-–Ba^{2+}–$[O_s–NO]^-$ (Fig. 2, middle and bottom panels). The existence of a NO_3^- at the cluster implies a disproportionation reaction. Here we did not consider the reaction pathway for this reaction. The structure including an ionic nitrate (Fig. 2, bottom panel) represents the ground state with a binding energy of 2.29 eV per NO_2. Our calculations demonstrate that the corresponding isomers with the nitrate in monodentate (Fig. 2, top panel) or bridging (Fig. 2, middle panel) configuration have similar binding energies of 0.7 and 0.8 eV above the ground state, respectively.

In the next step, we compared the calculated vibrational spectra with the experimental results. According to our calculations, one peak corresponding to the asymmetric stretching mode should appear at 1200 cm^{-1} when NO_2 is adsorbed above the cluster. This value is in good agreement with the experimentally observed band in the range of 1200–1250 cm^{-1}. The symmetric mode is expected at ∼1280 cm^{-1} in this case, but with a very weak intensity. For the configuration with NO_2 located in the $(BaO)_9$ cluster, theory predicts two peaks of similar intensity.

When comparing the calculated spectra with the IRAS experiment, we must take into account the fact that the experimental intensities will depend not only on the absolute value of the dynamic dipole moment (as yielded by the calculation), but also on its orientation with respect to the surface. Because the model surface is supported on a metal substrate [NiAl(110) in the present case], the parallel component of the dynamic

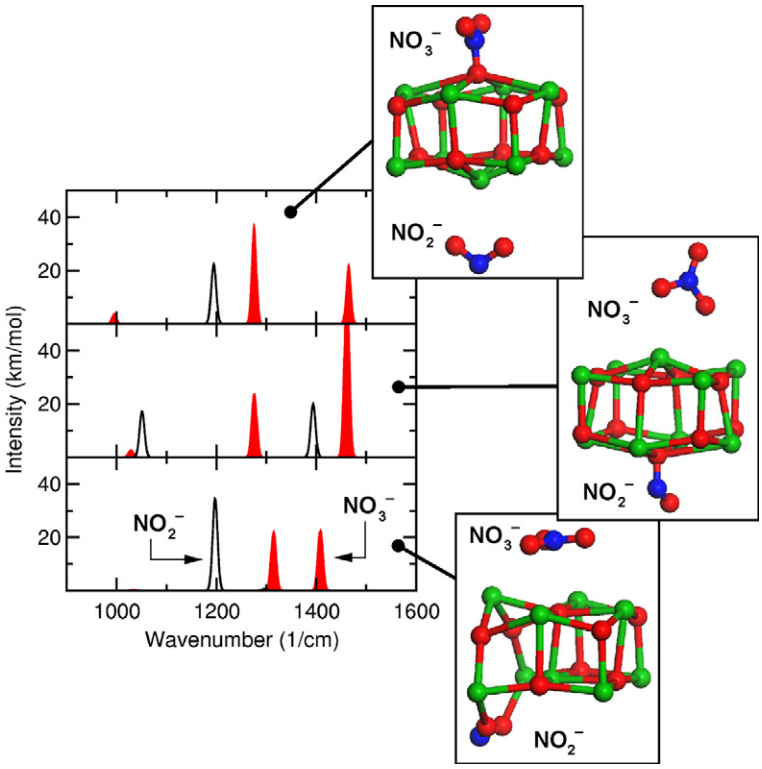

Fig. 2. Calculated vibrational spectra together with structural models. The vibrational modes are broadened by a Gaussian profile. Features corresponding to nitrate vibrations are colored. Atomic color code: oxygen (red), nitrogen (blue) and barium (green). (For interpretation of the references to color in this figure legend, the reader in referred to the web version of this article.)

dipole moment largely screens the conduction electrons. Consequently, the metal surface selection rule (MSSR) holds [29], stating that only the perpendicular component of the dynamic dipole moment will give rise to an absorption band. Taking this into account can explain the low intensity of the nitrite bands, assuming that the NO_2 is preferentially oriented parallel to the surface (compare Fig. 2, top panel). In this case, the asymmetric stretching mode would be largely polarized parallel, and thus the corresponding band would appear very weak on IRAS (see discussion in [49]).

Regarding the surface nitrates, we already mentioned that the NO_3^- ion has a twofold degenerate asymmetric stretching vibration in the gas phase. At the surface of the cluster, this degeneracy is lifted, and two features appear. For the ionic nitrate, the splitting was calculated to be $\sim$100 cm^{-1}. In the case of monodentate or bridging adsorption, however, the splitting was very similar; for both cases, it was $\sim$200 cm^{-1}, with one peak at 1275 cm^{-1} and the other peak at 1460 cm^{-1}. These results demonstrate the drawbacks to assigning vibrational features based solely on frequency positions. Only the ionic adsorption configuration can be unambiguously identified from the frequency positions of the vibrational bands.

Whereas our calculations demonstrate that clear identification of bridging and monodentate nitrates based solely on the position of the vibrational bands is not possible, the same calculations suggest a possible alternative strategy for experimentally differentiating the two species. At this point, the key issue is polarization of the modes with respect to the oxide surface, as illustrated in Fig. 3. Here the different normal modes are depicted schematically, including the orientation of the dynamic dipole moments. Both monodentate and bridging nitrates on BaO give rise to two components of the split $\nu_{as}(NO_3^-)$ mode located around 1300 and 1450 cm^{-1}; however, the polarization of the two components with respect to the oxide surface differs for the two surface species. For the monodentate, the low-frequency component is polarized perpendicular to the surface, and the high-frequency component is polarized parallel to the surface. The situation reversed for the bridging nitrate, with the low-frequency component showing parallel polarization and the high-frequency component demonstrating perpendicular polarization.

Whereas for powder catalysts, determining the orientation of the dynamic dipole moment may not be straightforward, this is easily done in a metal-supported model system, as considered here (see Fig. 3). As mentioned earlier, screening of the parallel components of the electrical field and the dynamic dipole moment in the metal-supported system gives rise to the MSSR [29], which states that only the perpendicular components of the dynamic dipole moment can be observed in IRAS. Because of the thinness of the oxide film, the MSSR strictly holds in the present case. If we now assume that the BaO particles are rather flat (as was suggested by STM; see above), we can expect the majority of surface nitrate species to be preferentially aligned upright with respect to the macroscopic sample surface. Based on this argument, the low-frequency component of $\nu_{as}(NO_3^-)$ for a monodentate would be allowed by the MSSR, whereas the high-frequency component would be forbidden. This situation would be reversed for the bridg-

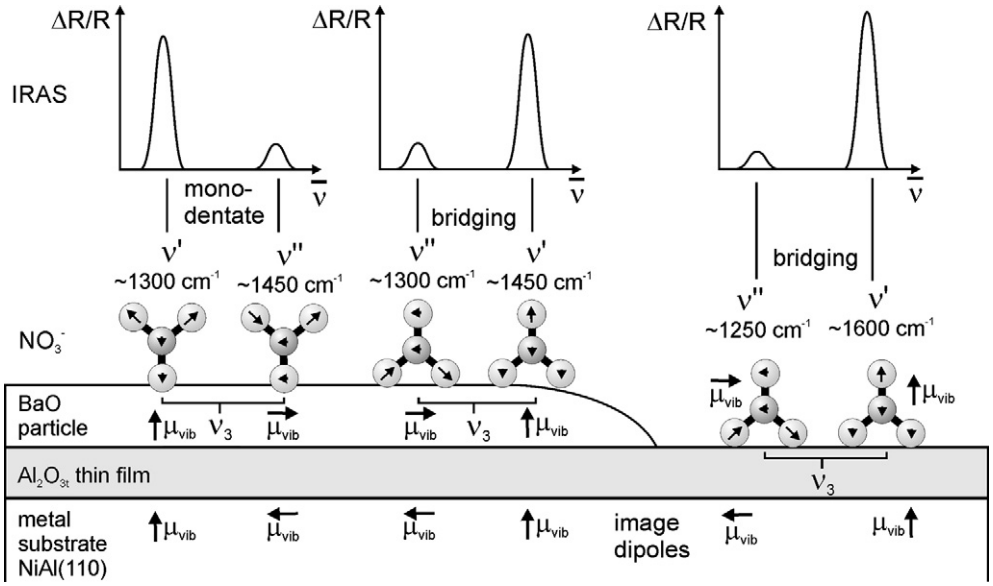

Fig. 3. Schematic representation of the two normal modes ν' and ν'', generated by lifting the degeneracy of the asymmetric stretching mode $\nu_{as}(NO_3^-)$ upon interaction of the nitrate ion with the surface. The two modes show different polarization with respect to the oxide surface. For an IRAS experiment on a flat metal supported model surface, the modes showing parallel polarization are largely screened by the substrate, whereas perpendicular modes are amplified. As a result different intensity patterns are expected for the monodentate and the bridging nitrate species (see text for discussion).

ing nitrate. Taking into account some imperfect alignment due to surface roughness, the forbidden bands may gain some finite intensity, but in general they should remain weak. In the present case, the effect is further amplified by characteristic differences in the dynamic dipole moment of the two components, as shown by the DFT calculations (see Fig. 2). The dynamic dipole moment for the 1280 cm^{-1} mode is strongest for monodentate adsorption, whereas the 1450 cm^{-1} mode shows the highest intensity for the bridging configuration. As a result, the spectral signature should be very different for the bridging and monodentate nitrate, with the high-frequency component dominating for the bridging species and the low-frequency component dominating for the monodentate. Similar arguments would be expected to hold for the nitrate species on Al_2O_3.

With this argument in mind, we reconsider the spectra shown in Fig. 1. For NO_2 on Al_2O_3, the two high-frequency components at 1590 and 1650 cm^{-1} strongly dominate over the two low-frequency features. Accordingly, we conclude that both types of surface nitrates on the Al_2O_3 support can be identified as bridging nitrates. This assignment is in accordance with some recent studies [18], whereas other authors have suggested the formation of monodentate nitrates as well [15,16,23,45]. The two pairs of bands at 1255/1590 cm^{-1} and 1297/1650 cm^{-1} appear sequentially and thus may be tentatively attributed to surface sites with different reactivity, such as defect sites (antiphase domain boundaries; see above) and regular terraces sites.

The nitrate on BaO exhibits a completely different behavior. Depending on particle size and reaction conditions, either the low-frequency component at around 1320 cm^{-1} or the high-frequency component at around 1450 cm^{-1} may completely dominate the spectrum. We conclude that both monodentate nitrates and bridging nitrates can be formed on BaO. Taking into account the intensity ratios, the following trends can be identified: At low temperature and low NO_2 exposure, monodentate nitrates are preferentially formed. With increasing NO_2 exposure, increasing BaO particle size, and increasing reaction temperature, the fraction of bridging nitrates increases. For larger BaO particles at elevated reaction temperatures, bridging nitrates become the dominating species. These trends are not reflected by any characteristic shifts in band positions, however.

The foregoing conclusion clearly contradicts some of the "traditional" assignments of the corresponding bands. In many cases, nitrate bands on BaO-containing samples have been attributed to monodentate species; for example, Sedlmair et al. assigned bands at around 1330 and 1430 cm^{-1} formed by NO_2 exposure of a commercial NSR catalyst ($Pt/BaO/Al_2O_3$) to monodentate nitrates [18], and Westerberg and Fridell assigned bands at 1290 and 1540 cm^{-1} to a monodentate species [15]. In those cases, in which a relatively large splitting between both components of $\nu_{as}(NO_3^-)$ were observed, the corresponding species were assigned to bidentates or bridging nitrates (bands at 1298 and 1583 cm^{-1} [23] and at 1214 and 1573 cm^{-1} [15]). As demonstrated by previous DFT calculations [21], our findings indicate that these assignments may need to be revised in the future. Clearly, the aforementioned and other detailed assignments, which are based solely on IR band positions, need to be verified by independent experiments.

4. Conclusion

We have combined DFT calculations and IRAS measurements on model NO_x storage systems to identify the types of surface nitrates formed on reaction of NO_2 with BaO/Al_2O_3 and Al_2O_3. Our calculations suggest the infeasibility of attempting to unambiguously identify the coordination geometry (i.e., monodentate nitrates and bridging nitrates) based solely on their vibrational frequencies. However, the polarization of

the NO-stretching modes provides independent information on the nature of the species. For metal-supported thin-film model systems, this information on the polarization of the modes is readily accessible experimentally, facilitating unambiguous identification.

Applying these arguments, we have demonstrated that bridging nitrates are formed predominately on the Al_2O_3 support, whereas both monodentate and bridging nitrates can be present on BaO. The ratio of the two species depends on the BaO particle size, the NO_2 exposure, and the reaction temperature. Whereas monodentate nitrates are initially formed at low exposure and low reaction temperature, bridging nitrates dominate on larger particles and at elevated reaction temperatures. Our proposed method provides an independent pathway to verify previous assignments of IR bands based solely on the frequency of the vibrational modes.

Acknowledgments

This work was performed in cooperation with and supported by Umicore Gmbh & Co KG (Automotive Catalysts). Financial support was provided by the Deutsche Forschungsgemeinschaft (DFG), the European Union (COST D-41), the DAAD, the Fonds der Chemischen Industrie (FCI), and the "Zerweck Fonds" (Universitätsbund Erlangen-Nürnberg). The work at the Competence Centre of Catalysis was supported by the Swedish Energy Agency and the member companies AB Volvo, Volvo Car Corporation, Scania CV AB, GM Powertrain Sweden AB, Haldor Topsoe A/S, and the Swedish Space Corporation. The authors thank Zhihui Qin, Shamil Shaikhutdinov, and Hans-Joachim Freund of FHI Berlin for providing the STM images and facilities and Karsten Meyer, Matthias Moll, Marc Gärtner, and Carola Vogel of the University of Erlangen for the use of their glove box facilities.

References

[1] J. Ryczkowsky, Catal. Today 68 (2001) 263.
[2] J. Libuda, Surf. Sci. 587 (2005) 55.
[3] M. Bäumer, J. Libuda, K.M. Neyman, N. Rosch, G. Rupprechter, H.-J. Freund, Phys. Chem. Chem. Phys. 9 (2007) 3541.
[4] W.S. Brown, D.A. King, J. Phys. Chem. B 104 (2000) 2578.
[5] K.I. Hadjiivanov, Catal. Rev. Sci. Eng. 42 (2000) 71.
[6] I.V. Yudanov, R. Sahnoun, K.M. Neyman, N. Rösch, J. Hoffmann, S. Schauermann, V. Johánek, H. Unterhalt, G. Rupprechter, J. Libuda, H.-J. Freund, J. Phys. Chem. B 107 (2003) 255.
[7] K. Hadjiivanov, V. Bushev, M. Kantcheva, D. Klissurski, Langmuir 10 (1994) 464.
[8] W.S. Kijlstra, D.S. Brands, E.K. Poels, A. Bliek, J. Catal. 171 (1997) 208.
[9] M.A. Hitchman, G.L. Rowbottom, Coord. Chem. Rev. 42 (1982) 55.
[10] D. Loffreda, D. Simon, P. Sautet, Chem. Phys. Lett. 291 (1998) 15.
[11] T. Gießel, O. Schaff, C.J. Hirschmugl, V. Fernandez, K.-M. Schindler, A. Theobald, S. Bao, R. Lindsay, W. Berndt, A.M. Bradshaw, C. Baddeley, A.F. Lee, R.M. Lambert, D.P. Woodruff, Surf. Sci. 406 (1998) 90.
[12] N. Takahashi, H. Shinjoh, T. Iijima, T. Suzuki, K. Yamazaki, K. Yokota, H. Suzuki, N. Miyoshi, S. Matsumoto, T. Tanizawa, T. Tanaka, S. Tateishi, K. Kasahara, Catal. Today 27 (1996) 63.
[13] W.S. Epling, L.E. Campbell, A. Yezerets, N.W. Currier, J.E. Parks II, Catal. Rev. 46 (2004) 163.
[14] E. Fridell, M. Skoglundh, B. Westerberg, S. Johansson, G. Smedler, J. Catal. 183 (1999) 196.
[15] B. Westerberg, E. Fridell, J. Mol. Catal. A Chem. 165 (2001) 249.
[16] F. Prinetto, G. Ghiotti, I. Nova, L. Lietti, E. Tronconi, P. Forzatti, J. Phys. Chem. B 105 (2001) 12732.
[17] C. Hess, J.H. Lunsford, J. Phys. Chem. B 106 (2002) 6358.
[18] C. Sedlmair, K. Seshan, A. Jentys, J.A. Lercher, J. Catal. 214 (2003) 308.
[19] I. Nova, L. Castoldi, F. Prinetto, V. DalSanto, L. Lietti, E. Tronconi, P. Forzatti, G. Ghiotti, R. Psaro, S. Recchia, Top. Catal. 30/31 (2004) 181.
[20] C. Paze, G. Gubitosa, S.O. Giacone, F.X. Llabres i Xamena, A. Zecchina, Top. Catal. 30/31 (2004) 169.
[21] P. Broqvist, H. Grönbeck, E. Fridell, I. Panas, J. Phys. Chem. B 108 (2004) 3523.
[22] A. Tsami, F. Grillo, M. Bowker, R.M. Nix, Surf. Sci. 600 (2006) 3403.
[23] T. Szailer, J.H. Kwak, D.H. Kim, J.C. Hanson, C.H.F. Peden, J. Szanyi, J. Catal. 239 (2006) 51.
[24] M. Piacentini, R. Stroebel, M. Maciejewski, S.E. Pratsinis, A. Baiker, J. Catal. 243 (2006) 43.
[25] F. Rohr, S.D. Peter, E. Lox, M. Kögel, A. Sassi, L. Juste, C. Rigaudeau, G. Belot, P. Gelin, M. Primet, Appl. Catal. B Environ. 56 (2005) 201.
[26] L. Castoldi, R. Matarrese, L. Lietti, P. Forzatti, Appl. Catal. B Environ. 64 (2006) 25.
[27] R.G. Tonkyn, R.S. Disselkamp, C.H.F. Peden, Catal. Today 114 (2006) 94.
[28] J. Dawody, I. Tonnies, E. Fridell, M. Skoglundh, Top. Catal. 42–43 (2007) 183.
[29] F.M. Hoffmann, Surf. Sci. Rep. 3 (1983) 107.
[30] R.M. Jaeger, H. Kuhlenbeck, H.-J. Freund, M. Wuttig, W. Hoffmann, R. Franchy, H. Ibach, Surf. Sci. 259 (1991) 235.
[31] J. Libuda, F. Winkelmann, M. Bäumer, H.-J. Freund, T. Bertrams, H. Neddermeyer, K. Müller, Surf. Sci. 318 (1994) 61.
[32] G. Kresse, M. Schmid, E. Napetschnig, M. Shishkin, L. Köhler, P. Varga, Science 308 (2005) 1440.
[33] M. Schmid, M. Shishkin, G. Kresse, E. Napetschnig, P. Varga, M. Kulawik, N. Nilius, H.-P. Rust, H.-J. Freund, Phys. Rev. Lett. 97 (2006) 046101.
[34] A. Desikusumastuti, M. Laurin, M. Happel, Z. Qin, S. Shaikhutdinov, J. Libuda, Catal. Lett. 121 (2008) 311.
[35] A. Desikusumastuti, T. Staudt, M. Happel, M. Laurin, J. Libuda, submitted for publication.
[36] R.J. Zollweg, Phys. Rev. 100 (1955) 671.
[37] E. Ozensoy, C.H.F. Peden, J. Szanyi, J. Phys. Chem. B 110 (2006) 17009.
[38] J. Perdew, K. Burke, M. Ernzerhof, Phys. Rev. Lett. 77 (1996) 3865.
[39] B. Delley, J. Chem. Phys. 92 (1990) 508.
[40] B. Delley, J. Chem. Phys. 113 (2000) 7758.
[41] B. Delley, Phys. Rev. B 66 (2002) 155125.
[42] H. Grönbeck, P. Broqvist, I. Panas, Surf. Sci. 600 (2006) 403.
[43] J. Hoffmann, S. Schauermann, J. Hartmann, V.P. Zhdanov, B. Kasemo, J. Libuda, H.-J. Freund, Chem. Phys. Lett. 354 (2002) 403.
[44] J. Szanyi, J.H. Kwak, R.J. Chimentao, C.H.F. Peden, J. Phys. Chem. C 111 (2007) 2661.
[45] A.L. Goodman, T.M. Miller, V.H. Grassian, J. Vac. Sci. Technol. A 16 (1998) 2585.
[46] P. Broqvist, H. Grönbeck, E. Fridell, I. Panas, J. Phys. Chem. B 106 (2002) 137.
[47] T. Venkov, K. Hadjiivanov, D. Klissurski, Phys. Chem. Chem. Phys. 4 (2002) 2443.
[48] E. Ozensoy, C.H.F. Peden, J. Szanyi, J. Phys. Chem. B 109 (2005) 15977.
[49] A. Desikusumastuti, M. Happel, K. Dumbuya, T. Staudt, M. Laurin, J.M. Gottfried, H.-P. Steinrück, J. Libuda, J. Phys. Chem. C, in press.